

Detectable molecular features above hydrocarbon haze via transmission spectroscopy with JWST:
Case studies of GJ 1214b-, GJ 436b-, HD 97658b-, and Kepler-51b-like planets

YUI KAWASHIMA,^{1,2,3} RENYU HU,^{4,5} AND MASAHIRO IKOMA^{3,6}

¹*SRON Netherlands Institute for Space Research, Sorbonnelaan 2, 3584 CA Utrecht, The Netherlands*

²*Earth-Life Science Institute, Tokyo Institute of Technology 2-12-1-IE-1 Ookayama, Meguro-ku, Tokyo 152-8550, Japan*

³*Department of Earth and Planetary Science, Graduate School of Science, The University of Tokyo, 7-3-1 Hongo, Bunkyo-ku, Tokyo 113-0033, Japan*

⁴*Jet Propulsion Laboratory, California Institute of Technology, 4800 Oak Grove Drive, Pasadena, CA 91109, USA*

⁵*Division of Geological and Planetary Sciences, California Institute of Technology, 1200 East California Boulevard, Pasadena, CA 91125, USA*

⁶*Research Center for the Early Universe (RESCEU), Graduate School of Science, The University of Tokyo, 7-3-1 Hongo, Bunkyo-ku, Tokyo 113-0033, Japan*

(Received; Revised; Accepted)

Submitted to ApJL

ABSTRACT

Some of the exoplanets so far observed show featureless or flat transmission spectra, possibly indicating the existence of clouds and/or haze in their atmospheres. Thanks to its large aperture size and broad wavelength coverage, JWST is expected to enable detailed investigation of exoplanet atmospheres, which could provide important constraints on the atmospheric composition obscured by clouds/haze. Here, we use four warm ($\lesssim 1000$ K) planets suitable for atmospheric characterization via transmission spectroscopy, GJ 1214b, GJ 436b, HD 97658b, and Kepler-51b, as examples to explore molecular absorption features detectable by JWST even in the existence of hydrocarbon haze in the atmospheres. We simulate photochemistry, the growth of hydrocarbon haze particles, and transmission spectra for the atmospheres of these four planets. Among the planetary parameters considered, super-Earths with hazy, relatively hydrogen-rich atmospheres are mostly expected to produce detectable molecular absorption features such as a quite prominent CH₄ feature at 3.3 μm even for the extreme case of the most efficient production of photochemical haze. For a planet that has extremely low gravity, such as Kepler-51b, haze particles grow significantly large in the upper atmosphere due to the small sedimentation velocity, resulting in the featureless or flat transmission spectrum in a wide wavelength range. This investigation shows that the transmission spectra with muted features measured by HST in most cases do not preclude strong features at the longer wavelengths accessible by JWST.

Keywords: planets and satellites: atmospheres — planets and satellites: composition — planets and satellites: individual (GJ 1214b, GJ 436b, HD 97658b, and Kepler-51b)

1. INTRODUCTION

Transmission spectra of close-in exoplanets observed so far are somewhat diverse (Sing et al. 2016). There are some studies that explored such diversity by examining the correlation between the observed amplitude of absorption features and the planetary proper-

ties (Stevenson 2016; Heng 2016; Crossfield & Kreidberg 2017). They all reached the conclusion that molecular absorption features are less pronounced in transmission spectra for lower equilibrium temperature although other planetary properties may affect such a correlation.

One explanation for this correlation is existence of photochemically-produced hydrocarbon haze obscuring the molecular features in the atmospheres of cooler planets (Zahnle et al. 2009; Miller-Ricci Kempton et al. 2012; Morley et al. 2013, 2015), because its primary

source CH_4 exists only at such low temperatures ($\lesssim 1000$ K) (e.g., Burrows & Sharp 1999).

Among stars hosting currently observable warm ($\lesssim 1000$ K) low-mass planets, GJ 1214, GJ 436, and HD 97658 are the only three host stars whose UV emission spectra have been observed (France et al. 2016; Youngblood et al. 2016; Loyd et al. 2016). Also, high-precision transmission spectra for their planets were observed with HST (e.g., Kreidberg et al. 2014; Knutson et al. 2014a,b). They all show flat or featureless transmission spectra between 1.1 and 1.7 μm , possibly indicating the existence of haze in the atmospheres. Since the knowledge of host-star’s UV spectrum is essential for the modeling of hydrocarbon haze (e.g., Kawashima & Ikoma 2018, 2019), the above three planets serve as the most promising targets to understand the nature of haze in exoplanet atmospheres. In addition, Kepler-51b is attracting attention as a favorable target for atmospheric characterization via transmission spectroscopy due to its extremely low density and large atmospheric scale height (Masuda 2014). In terms of haze science, this planet is also an interesting target because the sedimentation velocity of the particles in the atmosphere is expected to be quite low due to its low gravity, which allows particle growth in the upper atmosphere and mute features in the transmission spectrum. Recently, Wang & Dai (2019) investigated the effect of dusty outflows for Kepler-51b and 51d and showed that the existence of small dust of a fixed size at high altitudes could flatten the transmission spectra.

Currently, the number of exoplanets suitable for atmospheric characterization is still small due to the lack of bright targets and sufficient observational precision. Fortunately, TESS (Ricker et al. 2014) is expected to detect a great number of transiting exoplanets around nearby stars bright enough for atmospheric characterization. Also, JWST (Gardner et al. 2006) will enable high-precision transmission spectroscopy thanks to its large diameter, and also enable the spectroscopy at longer wavelengths than HST with its suite of spectroscopy instruments up to 12 μm , with photometry up to 28.5 μm (Beichman et al. 2014).

In this Letter, we use the above four favorable planets, GJ 1214b, GJ 436b, HD 97658b, and Kepler-51b, as examples and explore molecular absorption features detectable by JWST in the existence of hydrocarbon haze in their atmospheres. Planets similar in size to GJ 1214b and HD 97658b have been shown to be abundant (Fulton & Petigura 2018), indicating more planets in this size range will be found by TESS and will be the primary targets for atmospheric characterization by JWST (Louie et al. 2018). We describe the models in

§2, and show the results in §3. We discuss several effects to be examined in §4 and conclude this Letter in §5

2. METHOD

We model transmission spectra of an atmosphere with hydrocarbon haze using the photochemical, particle growth, and transmission spectrum models of Kawashima & Ikoma (2018) as follows: We first perform photochemical calculations to derive the steady-state, distribution of gaseous species. Our reaction rate list is the reduced version of Hu et al. (2012) and we include the reverse reactions in the same way as Hu & Seager (2014). Then we assume that the production rate of haze monomers at each altitude as the sum of the photodissociation rates of the major hydrocarbons in our photochemical model, CH_4 , HCN , and C_2H_2 , as an upper limit for the monomer production rate since this approach effectively assumes 100% conversion efficiency from the photodissociation of these hydrocarbons to haze monomers. With this assumption, we derive the steady-state distribution of haze particles by the particle growth calculations. Finally, we model transmission spectra of the atmospheres with the obtained distributions of haze particles and gaseous species. For the details of each of the three models, see Kawashima & Ikoma (2018).

As for the UV spectra of the host stars GJ 1214, GJ 436, and HD 97658, we use the data constructed by the MUSCLES Treasury Survey (France et al. 2016; Youngblood et al. 2016; Loyd et al. 2016). As for Kepler-51 whose UV spectrum has not been observed, because of its similar properties to the Sun, we use the solar spectrum from Segura et al. (2003)¹.

The setting for the atmospheres is as follows. We assume that the elemental abundance ratios of the atmospheric gas are the solar system ones, which we take from Table 2 of Lodders (2003). For the temperature-pressure profile, we use the analytical formula of Eq. (29) of Guillot (2010). We choose the values of the parameters, namely, the intrinsic temperature T_{int} , irradiation temperature T_{irr} , averaged opacity in the optical k_{ν} and that in the infrared k_{th} , so as to match the temperature-pressure profiles from Miller-Ricci & Fortney (2010) (the version with the solar metallicity and efficient dayside-to-nightside heat redistribution) for GJ 1214b and from Lewis et al. (2010) (their solar-metallicity version) for GJ 436b. As for HD 97658b and Kepler-51b, we adopt the same parameter values as the case of GJ 1214b except for T_{irr} , which we calculate with Eq. (1)

¹ http://vpl.astro.washington.edu/spectra/stellar/other_stars.htm

of Guillot (2010). We adopt the lower-boundary pressure of 1000 bar for photochemical calculation, while 10 bar in particle growth and transmission spectrum calculations.

For the calculations of photochemistry and particle growth, we choose the values of the reference radius equivalent to 1000 bar so as to roughly match the observed transit radii for a clear solar-composition atmosphere. Only for Kepler-51b, we use different values of the 1000-bar radius for two cases of the hazy and clear atmospheres. This is because with the same 1000-bar radius as in the clear atmosphere case, we would obtain too large transit radii for the hazy atmosphere to be consistent with the observed depth due to its extremely low gravity. When calculating the transmission spectra, we find the appropriate value of 10-bar radius that minimizes the reduced χ^2 value in comparison between the theoretical and observed transit depths. We consider the observed transmission spectra of Kreidberg et al. (2014), Knutson et al. (2014a), Knutson et al. (2014b) for GJ 1214b, GJ 436b, and HD 97658b, respectively, and the observed radius of Kepler-51b from Masuda (2014). For the calculation of theoretical transit depth for each observed data point, we consider the transmission curve of the filter used in the observation, taking those data from the SVO Filter Profile Service² (Rodrigo et al. 2012; Rodrigo & Solano 2013).

The parameters and their values we use are listed in Table 1.

3. RESULTS

Figure 1 shows the transmission spectrum models for atmospheres with and without haze for the cases of GJ 1214b, GJ 436b, HD 97658b, and Kepler-51b. We calculate the deviation in transit depth caused by nH_{ref} at a reference pressure level, R_{ref} , as $2nR_{\text{ref}}H_{\text{ref}}/R_s^2$ (Brown 2001), where H_{ref} is the atmospheric scale height at R_{ref} . The reference pressures are taken to be 10^{-4} bar for GJ 1214b, GJ 436b, and HD 97658b, and 10^{-6} bar for Kepler-51b, which roughly correspond to the pressure-levels of the transit radii. Note that the transmission spectrum models for clear atmospheres are also calculated with the distribution of gaseous species from photochemical calculations.

A number of spectral features are produced by molecules above the optically-thick photochemical haze. These features are generally $\lesssim 2$ atmospheric scale heights for GJ 1214b- and GJ 436b-like planets, and $\lesssim 1$ for HD 97658b-like planets, while $\lesssim 6$ for the cases of clear atmospheres. As photodissociation is the driver

for haze formation, this finding is general for exoplanets having solar composition atmospheres under similar levels of UV irradiation.

Considering a precision of ~ 25 ppm expected to be achieved by JWST (Beichman et al. 2014) and a spectral resolution of $R = 100$, we find detectable absorption features with the upper-limit production rate of haze monomers for each planet as listed in Table 2.

Some molecular absorption features will be detectable for a planet like GJ 1214b, due to lower incoming UV flux, namely lower monomer production rate, and larger planet-to-star radius ratio. For the planet GJ 1214b itself, however, the $1.4 \mu\text{m}$ H₂O feature was not detected by Kreidberg et al. (2014) at the precision of ~ 25 ppm. While Morley et al. (2015) demonstrated that their haze formation efficiency parameters of $\gtrsim 10\%$ could match the observed flatness of Kreidberg et al. (2014) for $50 \times$ Solar atmosphere, by considering particle growth, we have confirmed that our 1, 10, 100, $1000 \times$ Solar atmospheres all fail to become as flat as the observation even adopting the maximum monomer production rates (Kawashima & Ikoma 2019), possibly indicating extremely high metallicity, and/or aggregate haze particles (Adams et al. 2019), and/or coexistence of haze and other aerosols (see also discussion in §4). The message here is that a GJ 1214b-like planet having solar composition atmospheres and similar UV environment will be particularly suitable for future atmospheric characterization. For the case of HD 97658b, all the features in the wavelength range are undetectable due to the higher incoming UV flux, namely higher monomer production rate, and smaller planet-to-star radius ratio.

Among the detectable molecules, it is promising that several features of CH₄, which is a key indicator of haze formation, remains detectable even in the existence of haze for GJ 1214b- and GJ 436b-like planets, especially for its $3.3 \mu\text{m}$ feature. Note that this strong $3.3 \mu\text{m}$ CH₄ feature has been detected in the solar occultation spectrum of cooler celestial bodies in our solar system such as Saturn (Dalba et al. 2015) and Titan (Robinson et al. 2014). In the spectrum for Kepler-51b, the CH₄ features are invisible, because CH₄ is photodissociated and virtually absent above a thick haze layer at the low pressures of $\sim 10^{-6}$ bar.

In the case of Kepler-51b, the transmission spectrum model for the atmosphere with haze is quite featureless due to the existence of large haze particles in the upper atmosphere, unlike in the other three cases. However, distinct absorption features of CO₂ and CO are detectable due to their larger abundances in the upper atmosphere. This comes from its extremely low gravity, which makes an optical depth for a given pressure

² <http://svo2.cab.inta-csic.es/theory/fps/>

Table 1. Model parameters and their values used in the simulations

Parameter	Description	Value	Reference
Common parameters			
K_{zz}	Eddy diffusion coefficient	$1.00 \times 10^7 \text{ cm}^2 \text{ s}^{-1}$	
s_1	Monomer radius	$1.00 \times 10^{-3} \mu\text{m}$	
ρ_p	Particle internal density	1.00 g cm^{-3}	
GJ 1214b			
R_s	Host star radius	$0.201 R_\odot$	Anglada-Escudé et al. (2013)
M_p	Planet mass	$6.26 M_\oplus$	Anglada-Escudé et al. (2013)
$R_{1000 \text{ bar}}$	1000-bar radius	$2.07 R_\oplus$	
a	Semi-major axis	0.0148 AU	Anglada-Escudé et al. (2013)
d	Distance	14.6 pc	Youngblood et al. (2016)
T_{int}	Intrinsic temperature	120 K	
T_{irr}	Irradiation temperature	790 K	
k_v	Averaged opacity in the optical	$10^{-4.1} \text{ cm}^2 \text{ g}^{-1}$	
k_{th}	Averaged opacity in the infrared	$10^{-2.7} \text{ cm}^2 \text{ g}^{-1}$	
GJ 436b			
R_s	Host star radius	$0.464 R_\odot$	Torres et al. (2008)
M_p	Planet mass	$23.2 M_\oplus$	Torres et al. (2008)
$R_{1000 \text{ bar}}$	1000-bar radius	$3.758 R_\oplus$	
a	Semi-major axis	0.02872 AU	Torres et al. (2008)
d	Distance	10.1 pc	Youngblood et al. (2016)
T_{int}	Intrinsic temperature	170 K	
T_{irr}	Irradiation temperature	860 K	
k_v	Averaged opacity in the optical	$10^{-3.6} \text{ cm}^2 \text{ g}^{-1}$	
k_{th}	Averaged opacity in the infrared	$10^{-2.3} \text{ cm}^2 \text{ g}^{-1}$	
HD 97658b			
R_s	Host star radius	$0.703 R_\odot$	Dragomir et al. (2013)
M_p	Planet mass	$7.86 M_\oplus$	Dragomir et al. (2013)
$R_{1000 \text{ bar}}$	1000-bar radius	$1.943 R_\oplus$	
a	Semi-major axis	0.0796 AU	Dragomir et al. (2013)
d	Distance	21.1 pc	Youngblood et al. (2016)
T_{int}	Intrinsic temperature	120 K	
T_{irr}	Irradiation temperature	1037 K	
k_v	Averaged opacity in the optical	$10^{-4.1} \text{ cm}^2 \text{ g}^{-1}$	
k_{th}	Averaged opacity in the infrared	$10^{-2.7} \text{ cm}^2 \text{ g}^{-1}$	
Kepler-51b			
R_s	Host star radius	$0.940 R_\odot$	NASA Exoplanet Archive ^a
M_p	Planet mass	$2.1 M_\oplus$	Masuda (2014)
$R_{1000 \text{ bar}}$	1000-bar radius	$1.8 R_\oplus^b$	
a	Semi-major axis	0.2514 AU	Masuda (2014)
T_{int}	Intrinsic temperature	120 K	
T_{irr}	Irradiation temperature	793 K	
k_v	Averaged opacity in the optical	$10^{-4.1} \text{ cm}^2 \text{ g}^{-1}$	
k_{th}	Averaged opacity in the infrared	$10^{-2.7} \text{ cm}^2 \text{ g}^{-1}$	

^a<https://exoplanetarchive.ipac.caltech.edu>^bWe use the value of $2.3 R_\oplus$ for the clear atmosphere case

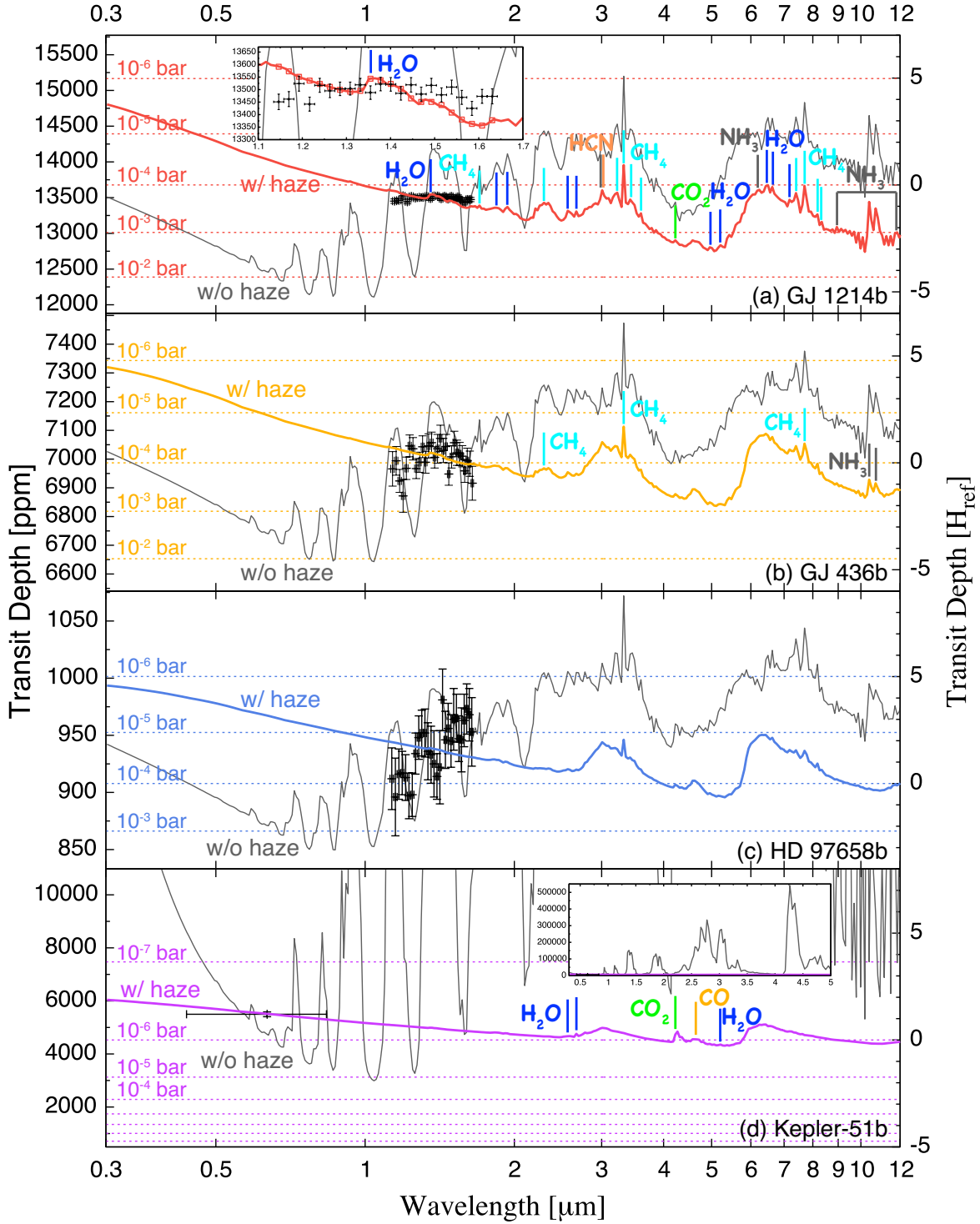


Figure 1. Transmission spectrum models for atmospheres with haze (thick color lines) and without haze (thin gray lines) for the cases of GJ 1214b (a), GJ 436b (b), HD 97658b (c), and Kepler-51b (d). This is in the order of the assumed total haze monomer production rate throughout the atmosphere, from the lowest panel to the highest panel, and reflects the amount of UV flux each planet receives. Those values are 1.38×10^{-12} , 7.83×10^{-12} , 5.45×10^{-11} , and 1.17×10^{-10} $\text{g cm}^{-2} \text{s}^{-1}$ for GJ 1214b, GJ 436b, HD 97658b, and Kepler-51b, respectively. The left vertical axes show the transit depths in ppm, while the right ones show those in atmospheric scale height at a certain pressure level for the hazy atmosphere cases (see the text for details). Horizontal dotted lines represent the transit depths corresponding to the pressure levels of every one order for the hazy atmosphere cases (see Eq. (67) of Kawashima & Ikoma (2018)). Additionally, zoomed-in and zoomed-out views are shown for GJ 1214b (a) and Kepler-51b (d), respectively. Observed transmission spectra of Kreidberg et al. (2014), Knutson et al. (2014a), and Knutson et al. (2014b) for GJ 1214b, GJ 436b, HD 97658b, respectively, and the observed radius of Kepler-51b from Masuda (2014) are also plotted with black points for reference. Note that horizontal error bars are the bandpasses or the FWHM of those used. The red points in the zoomed-in view for GJ 1214b (a) show the models binned at the observed bandpasses. The transmission spectrum models are smoothed with the spectral resolution of $R = 100$. Note the broad bumps at 3.0, 4.6, and 6.3 μm come from the absorption features of the tholin-like haze particles (Khare et al. 1984).

Table 2. Detectable absorption features by JWST

Planet Type	Molecules	Wavelength [μm]
GJ 1214b	H ₂ O	1.4, 1.8, 1.9, 2.6, 2.7, 5.0, 5.2, 6.5, 6.6, 7.2
	CH ₄	1.7, 2.3, 3.2, 3.3, 3.4, 3.6, 7.4, 7.7, 8.2, 8.3
	NH ₃	3.0, 6.2, 8.9-11.8
	HCN	3.0
	CO ₂	4.2
GJ 436b	CH ₄	2.3, 3.3, 7.7
	NH ₃	10.4, 10.7
HD 97658b	-	-
Kepler-51b	H ₂ O	2.6, 2.7, 5.2
	CO ₂	4.3
	CO	4.6

much larger and thus both the photodissociation rate of CH₄ and resultant production flux of atomic carbon much smaller. This very small production flux of C allows effective conversion of C into CO/CO₂ by reaction between H₂O, while C remains abundant and CO/CO₂ less abundant for the other planet cases.

In Figure 2, we plot the calculated vertical profiles of haze properties for the typical super-Earth gravity case of (a) HD 97658b and the extremely low gravity case of (b) Kepler-51b. In the case of HD 97658b, in the upper atmosphere ($\lesssim 10^{-6}$ bar), particles grow little because sedimentation occurs faster than collisional growth. Collisional growth occurs significantly from the pressure level of $\sim 10^{-6}$ bar on and results in haze particles with the average radius of $\sim 3 - 4 \mu\text{m}$ at the lower boundary of 10 bar. On the other hand, in the case of Kepler-51b, it is demonstrated that haze particles grow much larger in the upper atmosphere ($\sim 0.1 \mu\text{m}$ at $\sim 10^{-6}$ bar) and results in the particles of as large as $\sim 100 \mu\text{m}$ at 10 bar. This is because particles can become large via collisional growth even in the upper atmosphere, instead of falling downward rapidly, due to the small sedimentation velocity from low gravity. Note that although the monomer production rate for Kepler-51b is ~ 2 times higher than that for HD 97658b, the effect of the extremely low gravity turns out to make a much greater contribution to such a difference between those two spectra than that of high monomer production rate. Trends of vertical profiles for GJ 1214b and GJ 436b are similar to that of HD 97658b but with slightly smaller haze mass density because of the smaller monomer production rates (see Kawashima & Ikoma 2018, for the dependence on monomer production rate).

4. DISCUSSION

In this study, we have assumed maximum production rate of haze monomers in order to explore the detectable features at the worst case for solar composition atmospheres. As for the eddy diffusion coefficient, the molecular absorption features become more prominent for the larger value because of the efficient downward transport of haze particles, while remaining similar for the smaller value (Kawashima & Ikoma 2019).

In order to briefly assess the effect of metallicity and C/O ratio, in Figure 3, we show the transmission spectrum models for the cases of different metallicity and C/O ratio for GJ 1214b. One realizes that more absorption features become detectable for the case of $100 \times$ Solar atmosphere because of the smaller monomer production rate due to an enhanced photon-shielding effect by other molecules, while some features at relatively long wavelengths become undetectable due to smaller atmospheric scale height (Kawashima & Ikoma 2019). On the other hand, the effect of the C/O ratio is relatively small and among the detectable features for the solar composition atmosphere, H₂O features at 1.8, 5.0, 5.2, and 7.2 μm , CO₂ features at 4.2 μm , and NH₃ features at 6.2 μm become undetectable due to the slightly higher monomer production rate (Kawashima & Ikoma 2019).

Besides hydrocarbon haze, the existence of other aerosols can mute spectral features in transmission: condensation clouds such as KCl, ZnS, K₂SO₄, ZnO, and graphite clouds in the temperature range of interest in this study ($\lesssim 1000$ K) (Miller-Ricci Kempton et al. 2012; Morley et al. 2013; Mbarek & Kempton 2016; Ohno & Okuzumi 2018; Gao & Benneke 2018; Ormel & Min

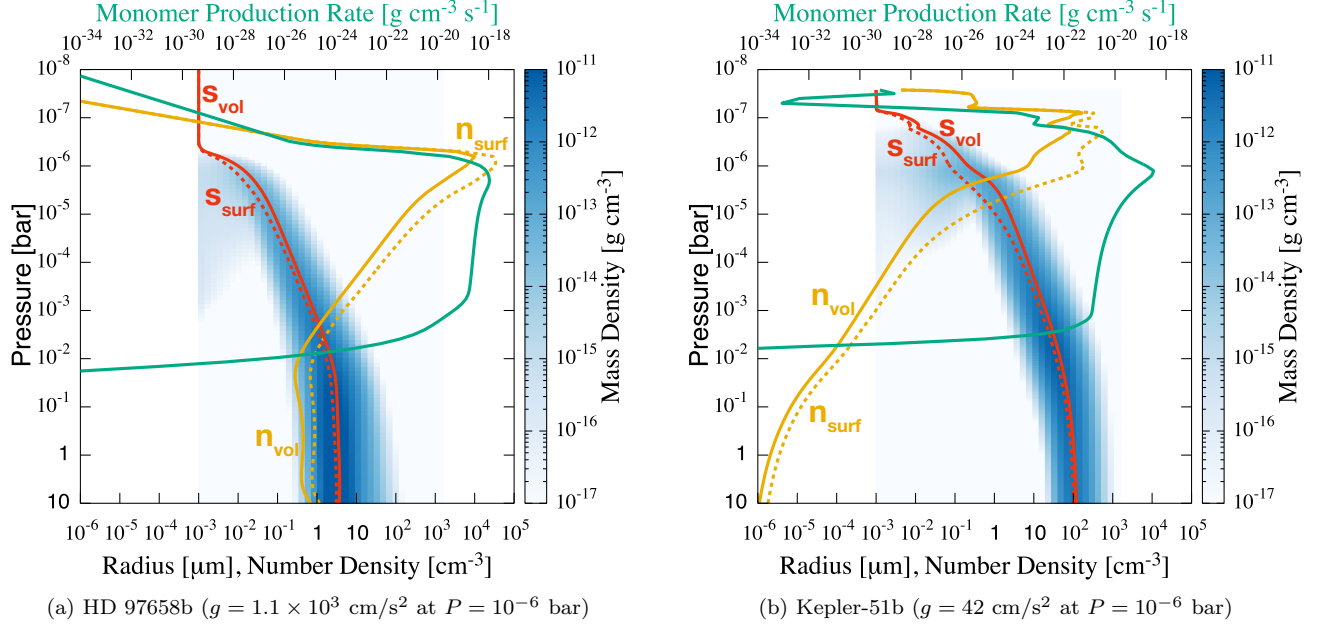


Figure 2. Vertical profiles of the properties of haze particles including the volume-average radius s_{vol} (red solid line) and number density n_{vol} (orange solid line), and the surface-average radius s_{surf} (red dashed line) and number density n_{surf} (orange dashed line), along with that of the monomer mass production rate (green solid line) for the cases of (a) HD 97658b and (b) Kepler-51b. See Kawashima & Ikoma (2018) for the definition of each quantity. The mass densities for all the size bins at each pressure level are also plotted with the blue color contour.

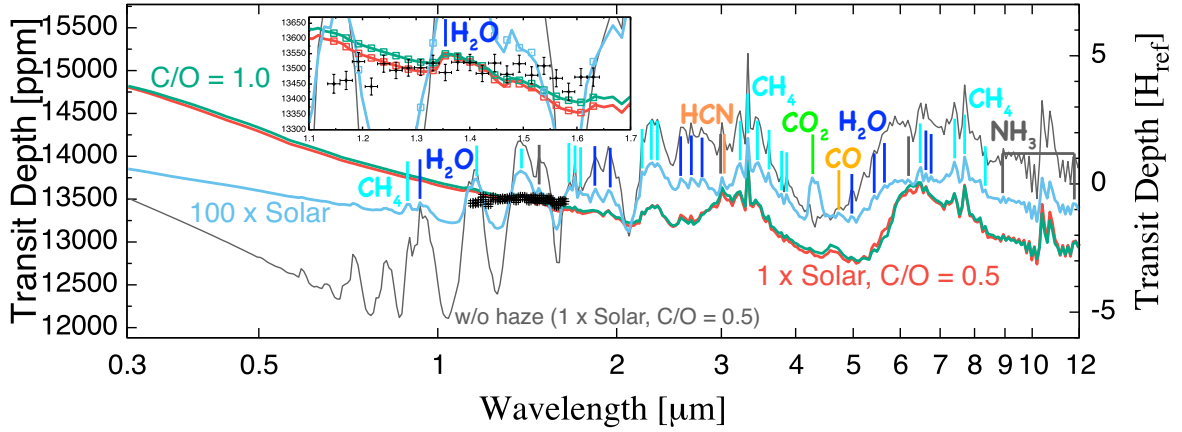


Figure 3. Same as Fig. 1 (a) but transmission spectrum models for the cases of $100 \times \text{Solar}$ (light blue line) and $\text{C/O} = 1.0$ (green line) atmospheres are also plotted. Detectable molecular absorption features for the case of $100 \times \text{Solar}$ atmosphere are labeled.

2019) and photochemical haze made of sulfur species (Hu et al. 2013; Zahnle et al. 2016; Gao et al. 2017).

In outflowing atmospheres, while having little effect on the profiles of pressure and density, the velocity of the outward flow may affect the sedimentation of small particles. The sedimentation velocity of haze particles are much faster than the outward velocity, which we estimate with the isothermal Parker solution (Parker 1958) for simplicity, for all the cases except Kepler-51b, whereas we have confirmed that in the case of Kepler-

51b, the sedimentation velocity of the volume-averaged-size particles are smaller than the outward velocity for the region of the pressures lower than $1.3 \times 10^{-7} \text{ bar}$. However, since the dominant monomer production region is below this pressure-level, the flow would have little impact on our results. The detailed consideration of this effect is beyond the scope of this study.

Also, as for extended atmospheres like Kepler-51b's, the effect of the tidal potential may affect the hydrostatic structure of the atmosphere. By using Eq. (12)

of Erkaev et al. (2007), we have confirmed that the gravitational potential at the optically thick radius at 1.0×10^{-6} bar, which is 9% of its Hill radius, would decrease to 86% due to the tidal potential and thus do not have significant impact on our results.

5. CONCLUSIONS

In this study, we have used four warm ($\lesssim 1000$ K) planets suitable for atmospheric characterization via transmission spectroscopy, GJ 1214b, GJ 436b, HD 97658b, and Kepler-51b, as examples and explored molecular absorption features detectable by JWST even in the existence of hydrocarbon haze in their atmospheres. Using the models of Kawashima & Ikoma (2018), we have simulated photochemistry, the growth of hydrocarbon haze particles, and transmission spectra for the atmospheres of these four planets.

We have found that among the planetary parameters considered, super-Earths with hazy, relatively hydrogen-rich atmospheres are mostly expected to produce detectable molecular absorption features such as a quite prominent CH_4 feature at $3.3 \mu\text{m}$ even for the extreme case of the most efficient production of photochemical haze. The sizes of those features correspond to $1 \sim 2$ atmospheric scale heights; while they are substantially smaller than a haze-free atmosphere, those features would be detectable with at precision expected for JWST. Especially, planets with higher gravity, lower UV irradiation, and higher temperature are more suitable (Kawashima & Ikoma 2019). Slight disagreement between our synthetic spectrum and very flat one observed for GJ 1214b, however, implies the importance of additional confounding effects.

We have also demonstrated that in the case of extremely low gravity planet, Kepler-51b, haze particles

grow significantly large in the upper atmosphere due to the small sedimentation velocity, resulting in the featureless or flat transmission spectrum in a wide wavelength range.

In summary, various molecular absorption features are expected to be detectable for relatively hydrogen-rich atmospheres even in the existence of hydrocarbon haze with JWST, given its high precision and long-wavelength capabilities. We thus suggest that the transmission spectra with muted features measured by HST in most cases do not preclude strong features at the longer wavelengths accessible by JWST.

We thank the anonymous referee for his/her careful reading and constructive comments, which helped us improve this letter greatly. The research was carried out at the Jet Propulsion Laboratory, California Institute of Technology, under a contract with the National Aeronautics and Space Administration. Y.K. thanks the travel support of JPL's Science Visitor and Colloquium Program. Y.K. is supported by the Grant-in-Aid for JSPS Fellow (JSPS KAKENHI No.15J08463), Leading Graduate Course for Frontiers of Mathematical Sciences and Physics, Grant-in-Aid for Scientific Research (A) (JSPS KAKENHI No.15H02065), and the European Union's Horizon 2020 Research and Innovation Programme under Grant Agreement 776403. R.H. is supported by NASA Grant No. 80NM0018F0612. M.I. is supported by JSPS KAKENHI No. 18H05439 and Core-to-Core Program International Network of Planetary Sciences. This work has made use of the MUSCLES Treasury Survey High-Level Science Products (doi:10.17909/T9DG6F) and the SVO Filter Profile Service (<http://svo2.cab.inta-csic.es/theory/fps/>) supported from the Spanish MINECO through grant AyA2014-55216.

REFERENCES

- Adams, D., Gao, P., de Pater, I., & Morley, C. V. 2019, *ApJ*, 874, 61, doi: [10.3847/1538-4357/ab074c](https://doi.org/10.3847/1538-4357/ab074c)
- Anglada-Escudé, G., Rojas-Ayala, B., Boss, A. P., Weinberger, A. J., & Lloyd, J. P. 2013, *A&A*, 551, A48, doi: [10.1051/0004-6361/201219250](https://doi.org/10.1051/0004-6361/201219250)
- Beichman, C., Benneke, B., Knutson, H., et al. 2014, *PASP*, 126, 1134, doi: [10.1086/679566](https://doi.org/10.1086/679566)
- Brown, T. M. 2001, *ApJ*, 553, 1006, doi: [10.1086/320950](https://doi.org/10.1086/320950)
- Burrows, A., & Sharp, C. M. 1999, *ApJ*, 512, 843, doi: [10.1086/306811](https://doi.org/10.1086/306811)
- Crossfield, I. J. M., & Kreidberg, L. 2017, *AJ*, 154, 261, doi: [10.3847/1538-3881/aa9279](https://doi.org/10.3847/1538-3881/aa9279)
- Dalba, P. A., Muirhead, P. S., Fortney, J. J., et al. 2015, *ApJ*, 814, 154, doi: [10.1088/0004-637X/814/2/154](https://doi.org/10.1088/0004-637X/814/2/154)
- Dragomir, D., Matthews, J. M., Eastman, J. D., et al. 2013, *ApJL*, 772, L2, doi: [10.1088/2041-8205/772/1/L2](https://doi.org/10.1088/2041-8205/772/1/L2)
- Erkaev, N. V., Kulikov, Y. N., Lammer, H., et al. 2007, *A&A*, 472, 329, doi: [10.1051/0004-6361:20066929](https://doi.org/10.1051/0004-6361:20066929)
- France, K., Parke Loyd, R. O., Youngblood, A., et al. 2016, *ApJ*, 820, 89, doi: [10.3847/0004-637X/820/2/89](https://doi.org/10.3847/0004-637X/820/2/89)
- Fulton, B. J., & Petigura, E. A. 2018, *AJ*, 156, 264, doi: [10.3847/1538-3881/aae828](https://doi.org/10.3847/1538-3881/aae828)
- Gao, P., & Benneke, B. 2018, *ApJ*, 863, 165, doi: [10.3847/1538-4357/aad461](https://doi.org/10.3847/1538-4357/aad461)

- Gao, P., Marley, M. S., Zahnle, K., Robinson, T. D., & Lewis, N. K. 2017, *AJ*, 153, 139, doi: [10.3847/1538-3881/aa5fab](https://doi.org/10.3847/1538-3881/aa5fab)
- Gardner, J. P., Mather, J. C., Clampin, M., et al. 2006, *SSRv*, 123, 485, doi: [10.1007/s11214-006-8315-7](https://doi.org/10.1007/s11214-006-8315-7)
- Guillot, T. 2010, *A&A*, 520, A27, doi: [10.1051/0004-6361/200913396](https://doi.org/10.1051/0004-6361/200913396)
- Heng, K. 2016, *ApJL*, 826, L16, doi: [10.3847/2041-8205/826/1/L16](https://doi.org/10.3847/2041-8205/826/1/L16)
- Hu, R., & Seager, S. 2014, *ApJ*, 784, 63, doi: [10.1088/0004-637X/784/1/63](https://doi.org/10.1088/0004-637X/784/1/63)
- Hu, R., Seager, S., & Bains, W. 2012, *ApJ*, 761, 166, doi: [10.1088/0004-637X/761/2/166](https://doi.org/10.1088/0004-637X/761/2/166)
- . 2013, *ApJ*, 769, 6, doi: [10.1088/0004-637X/769/1/6](https://doi.org/10.1088/0004-637X/769/1/6)
- Kawashima, Y., & Ikoma, M. 2018, *ApJ*, 853, 7, doi: [10.3847/1538-4357/aaa0c5](https://doi.org/10.3847/1538-4357/aaa0c5)
- . 2019, *ApJ*, submitted
- Khare, B. N., Sagan, C., Arakawa, E. T., et al. 1984, *Icarus*, 60, 127, doi: [10.1016/0019-1035\(84\)90142-8](https://doi.org/10.1016/0019-1035(84)90142-8)
- Knutson, H. A., Benneke, B., Deming, D., & Homeier, D. 2014a, *Nature*, 505, 66, doi: [10.1038/nature12887](https://doi.org/10.1038/nature12887)
- Knutson, H. A., Dragomir, D., Kreidberg, L., et al. 2014b, *ApJ*, 794, 155, doi: [10.1088/0004-637X/794/2/155](https://doi.org/10.1088/0004-637X/794/2/155)
- Kreidberg, L., Bean, J. L., Désert, J.-M., et al. 2014, *Nature*, 505, 69, doi: [10.1038/nature12888](https://doi.org/10.1038/nature12888)
- Lewis, N. K., Showman, A. P., Fortney, J. J., et al. 2010, *ApJ*, 720, 344, doi: [10.1088/0004-637X/720/1/344](https://doi.org/10.1088/0004-637X/720/1/344)
- Lodders, K. 2003, *ApJ*, 591, 1220, doi: [10.1086/375492](https://doi.org/10.1086/375492)
- Louie, D. R., Deming, D., Albert, L., et al. 2018, *PASP*, 130, 044401, doi: [10.1088/1538-3873/aaa87b](https://doi.org/10.1088/1538-3873/aaa87b)
- Loyd, R. O. P., France, K., Youngblood, A., et al. 2016, *ApJ*, 824, 102, doi: [10.3847/0004-637X/824/2/102](https://doi.org/10.3847/0004-637X/824/2/102)
- Masuda, K. 2014, *ApJ*, 783, 53, doi: [10.1088/0004-637X/783/1/53](https://doi.org/10.1088/0004-637X/783/1/53)
- Mbarek, R., & Kempton, E. M.-R. 2016, *ApJ*, 827, 121, doi: [10.3847/0004-637X/827/2/121](https://doi.org/10.3847/0004-637X/827/2/121)
- Miller-Ricci, E., & Fortney, J. J. 2010, *ApJL*, 716, L74, doi: [10.1088/2041-8205/716/1/L74](https://doi.org/10.1088/2041-8205/716/1/L74)
- Miller-Ricci Kempton, E., Zahnle, K., & Fortney, J. J. 2012, *ApJ*, 745, 3, doi: [10.1088/0004-637X/745/1/3](https://doi.org/10.1088/0004-637X/745/1/3)
- Morley, C. V., Fortney, J. J., Kempton, E. M.-R., et al. 2013, *ApJ*, 775, 33, doi: [10.1088/0004-637X/775/1/33](https://doi.org/10.1088/0004-637X/775/1/33)
- Morley, C. V., Fortney, J. J., Marley, M. S., et al. 2015, *ApJ*, 815, 110, doi: [10.1088/0004-637X/815/2/110](https://doi.org/10.1088/0004-637X/815/2/110)
- Ohno, K., & Okuzumi, S. 2018, *ApJ*, 859, 34, doi: [10.3847/1538-4357/aabee3](https://doi.org/10.3847/1538-4357/aabee3)
- Ormel, C. W., & Min, M. 2019, *A&A*, 622, A121, doi: [10.1051/0004-6361/201833678](https://doi.org/10.1051/0004-6361/201833678)
- Parker, E. N. 1958, *ApJ*, 128, 664, doi: [10.1086/146579](https://doi.org/10.1086/146579)
- Ricker, G. R., Winn, J. N., Vanderspek, R., et al. 2014, in *Proc. SPIE*, Vol. 9143, Space Telescopes and Instrumentation 2014: Optical, Infrared, and Millimeter Wave, 914320
- Robinson, T. D., Maltagliati, L., Marley, M. S., & Fortney, J. J. 2014, *Proceedings of the National Academy of Science*, 111, 9042, doi: [10.1073/pnas.1403473111](https://doi.org/10.1073/pnas.1403473111)
- Rodrigo, C., & Solano, E. 2013, Filter Profile Service Access Protocol Version 1.0, IVOA Note 10 May 2013
- Rodrigo, C., Solano, E., & Bayo, A. 2012, SVO Filter Profile Service Version 1.0, IVOA Working Draft 15 October 2012
- Segura, A., Krelove, K., Kasting, J. F., et al. 2003, *Astrobiology*, 3, 689, doi: [10.1089/153110703322736024](https://doi.org/10.1089/153110703322736024)
- Sing, D. K., Fortney, J. J., Nikolov, N., et al. 2016, *Nature*, 529, 59, doi: [10.1038/nature16068](https://doi.org/10.1038/nature16068)
- Stevenson, K. B. 2016, *ApJL*, 817, L16, doi: [10.3847/2041-8205/817/2/L16](https://doi.org/10.3847/2041-8205/817/2/L16)
- Torres, G., Winn, J. N., & Holman, M. J. 2008, *ApJ*, 677, 1324, doi: [10.1086/529429](https://doi.org/10.1086/529429)
- Wang, L., & Dai, F. 2019, *ApJL*, 873, L1, doi: [10.3847/2041-8213/ab0653](https://doi.org/10.3847/2041-8213/ab0653)
- Youngblood, A., France, K., Parke Loyd, R. O., et al. 2016, *ApJ*, 824, 101, doi: [10.3847/0004-637X/824/2/101](https://doi.org/10.3847/0004-637X/824/2/101)
- Zahnle, K., Marley, M. S., & Fortney, J. J. 2009, arXiv e-prints. <https://arxiv.org/abs/0911.0728>
- Zahnle, K., Marley, M. S., Morley, C. V., & Moses, J. I. 2016, *ApJ*, 824, 137, doi: [10.3847/0004-637X/824/2/137](https://doi.org/10.3847/0004-637X/824/2/137)